Spin Density Maps for the Ferrimagnetic Chain Compound $MnCu(pba)(H_2O)_3 \cdot 2H_2O$ (pba = 1,2-Propylenebis(oxamato)): Polarized Neutron Diffraction and Theoretical Studies

Valéry Baron,[†] Béatrice Gillon,*[,†] Alain Cousson,[†] Corine Mathonière,[‡] Olivier Kahn,*[,‡] André Grand,[‡] Lars Öhrström,[§] Bernard Delley,[⊥] Michel Bonnet,[||] and Jean-Xavier Boucherle[||]

Contribution from the Laboratoire Léon Brillouin, Centre d'Etudes Nucléaires de Saclay, 91191 Gif sur Yvette, France, Laboratoire des Sciences Moléculaires, Institut de Chimie de la Matière Condensée de Bordeaux, UPR CNRS n 9048, 33608 Pessac, France, Laboratoire de Chimie de Coordination, URA CNRS n 1195, and Département de Recherche Fondamentale sur la Matière Condensée, Centre d'Etudes Nucléaires de Grenoble, 38054 Grenoble, France, and Paul Scherrer Institute Zürich, Badenerstrasse 569, 8048 Zürich, Switzerland

Received December 3, 1996[⊗]

Abstract: This paper is devoted to the determination of the spin density in the ferrimagnetic ground state of the bimetallic chain compound $MnCu(pba)(H_2O)_3 \cdot 2H_2O$, with pba = 1,3-propylenebis(oxamato). The crystal structure, previously determined at room temperature through X-ray diffraction, was redetermined at 10 K through unpolarized neutron diffraction (orthorhombic system, space group *Pnma*, $a = 12.727(11)$ Å, $b = 21.352(19)$ Å, $c = 5.153(3)$ Å, $Z = 4$). The experimental spin density has been deduced from polarized neutron diffraction data recorded at 10 K under 50 kOe. Positive spin densities were observed on the manganese side and negative spin densities on the copper side. The delocalization of the spin density from the metal centers toward the oxamato bridging ligand was found to be more pronounced on the copper side than on the manganese side, so that the nodal surface (of zero spin density) is closer to manganese than to copper. The experimental spin distribution has been compared to the theoretical distributions deduced from density functional theory (DFT) calculations, using both DGauss and DMol programs. The experimental results for the title chain compound have also been compared to the spin distribution for the binuclear compound $[Mn(Me_6\text{-}[14]ane\text{-}N_4)Cu(oxpn)](CF_3SO_3)_2$ with Me_6-[14]ane-N_4 = (±)-5,7,7,12,14,14-hexamethyl-1,4,8,11-tetraazacyclotetradecane, and oxpn = *N*,*N*′-bis(3-aminopropyl)oxamido, recently reported. The most striking difference between pair and chain compounds concerns the positive P_+ and negative P_- spin populations carried by the manganese and copper sides, respectively. For the pair compound P_+ was found as 4.67(8) μ_B, and P_- as −0.67(8) μ_B while for the chain compound these values are 5.05(7) μ_B and −1.05(10) μ_B, respectively. The spin distribution for the ferrimagnetic chain compound is very close to a Neel state ($P_+ = 5\ \mu_B$ and $P_- = -1\ \mu_B$).

Introduction

The design of molecular compounds exhibiting a spontaneous magnetization below a certain critical temperature is probably the most active area of molecular magnetism. The very first compounds of this kind were reported in 1986.[1,2] The majority of molecular-based magnets reported so far are heterobimetallic species, in which different metal ions are bridged by extended bisbidentate ligands such as oxamato,[3−8] oxamido,[9,10] oxalato,[11−15] dithiooxalato,[16] or oximato.[17,18] The interaction between nearest neighbor spin carriers may be ferromagnetic; it may be antiferromagnetic as well with a noncompensation of the local spins. In this latter case the most favorable situation is that where the difference between the local spins $|S_A - S_B|$ is the largest, which is realized in Mn(II)Cu(II) compounds with S_{Mn}

[†] Centre d'Etudes Nucléaires de Saclay.
[‡] Institut de Chimie de la Matière Condensée de Bourdeaux.
[§] Laboratoire de Chimie de Coordination, Centre d'Etudes Nucleaires de Grenoble.
[⊥] Paul Scherrer Institute Zürich.
[||] Département de Recherche Fondamentale sur la Matière Condensée, Centre d'Etudes Nucléaires de Grenoble.
[⊗] Abstract published in *Advance ACS Abstracts,* April 1, 1997.

(1) Miller, J. S.; Calabrese, J. C.; Epstein, A. J.; Bigelow, R. W.; Zang, J. H.; Reiff, W. M. *J. Chem. Soc., Chem. Commun.* **1986**, 1026.
(2) Pei, Y.; Verdaguer, M.; Kahn, O.; Sletten, J.; Renard, J. P. *J. Am. Chem. Soc.* **1986**, *108*, 428.
(3) Kahn, O.; Pei, Y.; Verdaguer, M.; Renard, J. P.; Sletten, J. *J. Am Chem. Soc.* **1988**, *110*, 782.
(4) Nakatani, K.; Bergerat, P.; Codjovi, E.; Mathonière, C.; Pei, Y.; Kahn, O. *Inorg. Chem.* **1991**, *30*, 3977.
(5) Stumpf, H. O.; Pei, Y.; Kahn, O.; Sletten, J.; Renard, J. P. *J. Am. Chem. Soc.* **1993**, *115*, 6738.
(6) Stumpf, H. O.; Ouahab, L.; Pei, Y.; Grandjean, D.; Kahn, O. *Science* **1993**, *261*, 447.
(7) Stumpf, H. O.; Ouahab, L.; Pei, Y.; Bergerat, P.; Kahn, O. *J. Am. Chem. Soc.* **1994**, *116*, 3866.
(8) Stumpf, H. O.; Pei, Y.; Michaut, C.; Kahn, O.; Renard, J. P.; Ouahab, L. *Chem. Mater.* **1994**, *6*, 257.
(9) Pei, Y.; Kahn, O.; Nakatani, K.; Codjovi, E.; Mathonière, C.; Sletten, J. *J. Am. Chem. Soc.* **1991**, *113*, 6558.
(10) Nakatani, K.; Carriat, J. Y.; Journaux, Y.; Kahn, O.; Lloret, F.; Renard, J. P.; Pei, Y.; Sletten, J.; Verdaguer, M. *J. Am. Chem. Soc.* **1989**, *111*, 5739.
(11) Zhong, Z. J.; Matsumoto, H.; Okawa, H.; Kida, S. *Chem. Lett.* **1990**, 87.
(12) Tamaki, H.; Zhong, Z. J.; Matsumoto, N.; Kida, S.; Koikawa, M.; Achiwa, N.; Hashimoto, Y.; Okawa, H. *J. Am. Chem. Soc.* **1992**, *114*, 6974.
(13) Decurtins, S.; Schmalle, H. W.; Oswald, H. R.; Linden, A.; Ensling, J.; Gütlich, P.; Hauser, A. *Inorg. Chim. Acta* **1994**, *216*, 65.
(14) Okawa, H.; Mitsumi, M.; Ohba, M.; Kodera, M.; Matsumoto, N. *Bull Chem. Soc. Jpn.* **1994**, 67, 2139.
(15) Mathonière, C.; Nuttall, C. J.; Carling, S. G.; Day, P. *Inorg. Chem.* **1996**, *35*, 1201.
(16) Tamaki, H.; Mitsumi, M.; Nakamura, K.; Matsumoto, N.; Kida, S.; Okawa, H.; Iijima, S. *Chem. Lett.* **1992**, 1975. Decurtins, S.; Schmalle, H. W.; Pellaux, R.; Schneuwly, P.; Hauser, A. *Inorg. Chem.* **1996**, *35*, 1451.
(17) Lloret, F.; Ruiz, R.; Julve, M.; Faus, J.; Journaux, Y.; Castro, I.; Verdaguer, M. *Chem. Mater.* **1992**, *4*, 1150.
(18) Lloret, F.; Ruiz, R.; Cervera, B.; Castro, I.; Julve, M.; Faus, J.; Real, A.; Sapina, F.; Journaux, Y.; Colin, J. C.; Verdaguer, M. *J. Chem. Soc., Chem. Commun.* **1994**, *2615*.

S0002-7863(96)04162-5 CCC: $14.00

$= 5/2$ and $S_{Cu} = 1/2$ local spins. The first molecular-based heterobimetallic magnets were oxamato- and oxamido-bridged Mn(II)Cu(II) species.[3−10] Therefore, it was worthwhile to analyze the interaction between Mn(II) and Cu(II) ions through such an extended bridge in a thorough fashion. Polarized neutron diffraction (PND) is a unique tool for that. This technique is nowadays more and more applied to the field of molecular magnetism. It permits one to obtain the whole spin density distribution for a molecule or a molecular-based species in the solid state. In contrast, the magnetic resonance spectroscopies only provide partial information on the spin distribution. Let us note, however, that PND cannot be applied as systematically as magnetic resonance spectroscopies because of the necessity to use large single crystals.

In a recent paper we investigated the spin density distribution in the simplest case of Mn(II)Cu(II) heterobimetallics, i.e., a binuclear species.[19] The compound we selected was [Mn(Me_6-[14]ane-N_4)Cu(oxpn)](CF_3SO_3)$_2$, with Me_6-[14]ane-N_4 = (±)-5,7,7,12,14,14-hexamethyl-1,4,8,11-tetraazacyclotetradecane, and oxpn = *N*,*N*′-bis(3-aminopropyl)oxamido.[20] The experimental data deduced from polarized neutron diffraction were compared to the results of several theoretical approaches, corresponding to different levels of sophistication, which provided us some important insights on both spin delocalization and spin polarization. Here, we present the results obtained with the ferrimagnetic chain compound MnCu(pba)(H_2O)$_3$·2H_2O, with pba = 1,3-propylenebis(oxamato). The synthesis, room temperature crystal structure, and magnetic properties of MnCu(pba)(H_2O)$_3$·2H_2O have already been reported.[21] This compound may be considered as the archetype of a one-dimensional ferrimagnet.[22] The $\chi_M T$ versus T plot, χ_M being the molar magnetic susceptibility and T the temperature, presents a characteristic minimum around 120 K and increases very rapidly as T decreases further. The compound exhibits a long-range antiferromagnetic ordering of the ferrimagnetic chains at 2.3 K. The magnitude of the Mn(II)−Cu(II) intrachain interaction, J, was determined from the magnetic susceptibility data, using a model in which S_{Mn} is treated as a classical spin, and S_{Cu} as a quantum spin. J was found as -23.4 cm^{-1}, the spin Hamiltonian for the bimetallic chain being written down as $-J\sum_i(\mathbf{S}_{Mn,i}\cdot\mathbf{S}_{Cu,i} + \mathbf{S}_{Mn,i+1}\cdot\mathbf{S}_{Cu,i})$.

The present work enables for a direct comparison between the spin distribution in the oxamato-bridged Mn(II)Cu(II) linear chain compound and the discrete oxamido-bridged [Mn(cth)Cu(oxpn)](CF_3SO_3)$_2$ molecular species.[19] A preliminary report of this work has already appeared.[23] To the best of our knowledge only one chain compound has been the subject of such a spin density determination, namely Cu(hfac)$_2$NITMe with hfa = hexafluoroacetylacetone and NITMe = methyl nitronyl nitroxide, in which there is alternation of metal ions and organic radicals.[24]

The paper may be considered as the following of that concerning the Mn(II)Cu(II) pair,[19] which will be often referred to, and as much as possible we will try to avoid the duplication of information concerning either the PND technique or the calculation methods. In other terms, this paper is not entirely self-consistent. It supposes that the information reported in ref 19 is known. The manuscript is organized as follows: The first part is devoted to both the unpolarized and polarized neutron diffraction experiments, together with the determination of the nuclear structure and the spin density maps at 10 K. The second part is devoted to the theoretical discussion of the findings, using density functional theory (DFT) methods. Finally, the last part is devoted to a comparison between the spin distributions for the pair and chain compounds.

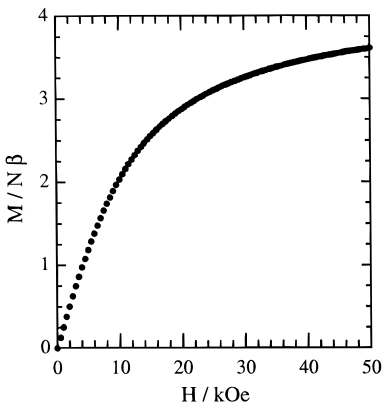

Figure 1. Field dependence of the magnetization in Bohr magneton units (Nβ) for MnCu(pba)(H_2O)$_3$·2H_2O at 10 K.

Experimental Section and Calculation Methods

Synthesis. Large single crystals (up to 14 mm^3) of MnCu(pba)(H_2O)$_3$·2H_2O were obtained by slow diffusion in a H-shaped tube at 50 °C of two 10^{-3} molar aqueous solutions containing Mn(II) perchlorate and Na_2[Cu(pba)]·3.5H_2O, respectively. The temperature, 50 °C, seems to play a crucial role as far as the size of the single crystals is concerned.

Magnetization. The field dependence of the magnetization was measured at 10 K with a Quantum Design MPMS-5S SQUID magnetometer working up to 50 kOe. The curve is shown in Figure 1.

Structure Determination at 10 K through Neutron Diffraction. The crystal structure of MnCu(pba)(H_2O)$_3$·2H_2O was already solved by X-ray diffraction at room temperature. The compound crystallizes in the centrosymmetric space group *Pnma*, with $Z = 4$. In order to determine the precise hydrogen positions and the low-temperature thermal parameters, a neutron diffraction experiment was carried out on the four-circle diffractometer at the reactor Siloé located in Grenoble (France). The main crystal data along with the experimental conditions are reported in Table 1. A single crystal of 14 mm^3 was set in a three stage Joule-Thompson refrigerator and cooled down to 10 K. The cell parameters were refined by least-squares fitting on 17 reflections. A first set of 422 reflections was measured. Afterwards, the crystal broke due to a rapid increase of temperature, and a second set of 273 unique reflections, including 123 reflections common to both sets, was collected with a piece of the crystal of 7 mm^3. A Lorentz correction was applied to the integrated intensities. Absorption corrections were performed using the program DISTA3 of the Cambridge Library package with a linear absorption coefficient of 2.10 cm^{-1}. The structural parameters were refined using the least-squares program CRYSTALS[25] and taking as starting parameters those obtained from the X-ray investigation.[21] Only 527 reflections with F greater than 3σ were taken into account to refine 182 parameters. A refinement on F with two blocks of parameters was performed. The first block contained one scale factor along with the extinction parameter and the thermal parameter, while the second block was constituted by all position parameters. All atoms were refined anisotropically. A weighting scheme using a Chebyshev polynomial was chosen. A goodness of fit $S = 1.18$ and agreement factors $R(F) = 0.047$ and $R_w(F) = 0.042$ were obtained. The extinction parameter g for isotropic extinction correction was refined, and a value of 0.014(3) was obtained, corresponding to a negligible correction.

(19) Baron, V.; Gillon, B.; Plantevin, O.; Cousson, A.; Mathonière, C.; Kahn, O.; Grand, A.; Öhrström, L.; Delley, B. *J. Am. Chem. Soc.* **1996**, *118*, 11822.

(20) Mathonière, C.; Kahn, O.; Daran, J. C.; Hilbig, H.; Köhler, F. H. *Inorg. Chem.* **1993**, *32*, 4057.

(21) Pei, Y.; Verdaguer, M.; Kahn, O.; Sletten, J.; Renard, J. P. *Inorg. Chem.* **1987**, *26*, 138.

(22) Kahn, O. *Molecular Magnetism*; VCH: New York, 1993.

(23) Baron V., Gillon B., Mathonière C., Kahn O., Bonnet M., Boucherle J. X. *Mol. Cryst. Liq. Cryst.* **1993**, *233*, 247.

(24) Ressouche, E.; Boucherle, J. X.; Gillon, B.; Rey, P.; Schweizer, J. *J. Am. Chem. Soc.* **1993**, *115*, 3610.

(25) Carruthers, J. R.; Watkin, D. J.; Betteridge, P. W. *CRYSTALS, an Advanced Crystallographic Program System*; University of Oxford: Oxford, England, 1988.

Table 1. Crystallographic and Experimental Data for the Structure Determination at 10 K

Crystallographic Data	
formula	$CuMnC_7H_{16}N_2O_{11}$
molar weight	422.68 g·mol^{-1}
space group	*Pnma*
system	orthorhombic
Z	4
density	2.00
Data Collection	
monochromator	Cu (220)
wavelength (Å)	1.183
T (K)	10
scan mode	ω-2θ
scan step (deg)	0.1
moniteur (cts per step)	100000
sin θ/λ(Å^{-1})	0.49
no. of reflcns for the cell refinement	17
crystal size (mm^3)	14, 7
no. of measd reflcns	422, 273
Conditions for Refinement	
no. of reflcns $N_o(F > 3\sigma)$	527
no. of parameters N_v	182
Agreement Factors[a]	
$R(F)$	0.047
$R_w(F)$	0.042
S	1.18

[a] $R(F) = (\Sigma_{hkl}||F_o| - |F_c||)/(\Sigma_{hkl}|F_o|)$, $R_w(F) = [(\Sigma_{hkl}w(|F_o| - |F_c|)^2/(\Sigma_{hkl}\, w|F_o|^2\,)]^{1/2}$, $S = [(\Sigma_{hkl}\, w(|F_o| - |F_c|)^2)/(N_o - N_c)\,]^{1/2}$, with N_o = number of reflections, N_v = number of parameters and w weighting scheme (Chebychev polynomial): $w = (\text{weight})(1 - (\delta F/6\sigma(F))^2)^2$ using parameters 6.72, −9.5, 4.36, −1.18, −0.775.

Table 2. Experimental Data Concerning the Polarized Neutron Measurements

Experimental Conditions		
monochromator	$Co_{0.92}Fe_{0.08}$ (200)	
wavelength (Å)	0.83	
beam polarization	0.920(4)	
flipping efficiency	1	
T (K)	10	
H (kOe)	50	
crystal size (mm^3)	14	
Data Collection		
vertical axis	*c*	*b*
no. of measd reflcns	220	85

Polarized Neutron Experiment. Two sets of data were collected on the polarized neutron diffractometer 5C1 of the L.L.B. at the Orphée reactor in Saclay on the single crystal of 14 mm^3 used afterwards for the nuclear structure determination. Table 2 presents the experimental conditions and information on data collection. The wavelength was 0.83 Å, and the polarization of the incident beam obtained with use of a $Co_{0.92}Fe_{0.08}$ monochromator was equal to 0.920(4). The sample was cooled down to 10 K, and a magnetic field of 50 kOe was applied in order to align the unpaired electron spins. The temperature of the experiment, 10 K, is just above the temperature range where the magnetic susceptibility is influenced by anisotropy effects.[26] The experimental magnetization at 10 K under 50 kOe is equal to 3.6 μ_B, which corresponds to 90% of the estimated saturation value $M_S = 4$ μ_B. In fact, M_S might be slightly different of 4 μ_B, due to the second-order orbital contribution in the Zeeman factor for Cu(II). On the other hand, the weak antiferromagnetic interchain interactions cannot influence the M_S value. Indeed, a weak external magnetic field is sufficient to overcome these interactions. The title compound may be considered as a metamagnet. The crystal was first set up in the superconducting cryomagnet with its *c* axis direction (corresponding to the long dimension of the crystal) vertical, and the flipping ratios of 220 independent *hkl* reflections with $l = 0$ to 2 were collected. In a second time the *b* axis direction (corresponding to the second largest dimension of the crystal) was set up vertically, and 85 *hkl* reflections with $k = 0$ to 20 were measured including 49 reflections common to both sets. No weak reflections were collected in order to avoid multipole scattering problems which could affect their measurements. Only reflections with $|F_N| > 3 \times 10^{-12}$ cm were taken into consideration. The magnetic structure factors were deduced from the experimental flipping ratios with the help of the low temperature nuclear structure factors, taking into account imperfect beam polarization and extinction corrections. The obtained F_M values were corrected for the contribution arising from the nuclear polarization of the hydrogen nuclear spins. In the experimental conditions of temperature and field the calculated value for the hydrogen nuclear spin polarization f^{H}_{NP} is 0.002 76 10^{-12} cm.

Density Functional Theory Calculations. The DFT calculations were performed with the DGauss 2.3[27,28] and DMol-DSolid 2.3.7[29,30] programs in the same way as described earlier.[19] All geometries were taken from the neutron diffraction structure. In the DGauss program,

Table 3. Cell Parameters, Intra- and Intermolecular Distances between Metal Ions, and Interatomic Distances (in Å) at 298 and 10 K

Cell Parameters (in Å)		
	($T = 298$ K)	($T = 10$ K)
a	12.945(1)	12.727(11)
b	21.250(4)	21.352(19)
c	5.2105(8)	5.153(5)
Intra- and Intermolecular Distances (in Å)		
	($T = 298$ K)	($T = 10$ K)
Mn···Cu intrachain	5.412	5.431(1)
Mn···Mn interchain	5.211	5.154
Interatomic distances (in Å)		
	($T = 298$ K)	($T = 10$ K)
Mn−O1	2.165(1)	2.170(4)
Mn−O2	2.169(1)	2.169(4)
Mn−O4	2.197(2)	2.189(4)
Cu−N1	1.933(1)	1.951(4)
Cu-O3	1.990(1)	1.988(5)
Cu-O5	2.281(2)	2.283(8)
O1-C2	1.278(2)	1.282(6)
O2−C1	1.245(2)	1.257(6)
O3-C1	1.260(2)	1.280(6)
N1-C2	1.285(2)	1.290(5)
C1-C2	1.538(3)	1.535(5)

Table 4. Atomic Coordinates and Equivalent Isotropic Displacements at 10 K

atoms	*x*	*y*	*z*	U_{eq} (Å^2)[a]
Cu	0.5504(3)	0.25	0.1488(9)	0.0038
Mn	0.5	0	0	0.0047
O1	0.4365(3)	0.0764(2)	0.229(1)	0.0101
O2	0.5960(3)	0.0784(2)	−0.1235(9)	0.0079
O3	0.6156(3)	0.1825(2)	−0.0623(9)	0.0052
O4	0.6177(3)	−0.0211(2)	0.297(1)	0.0062
O5	0.6739(4)	0.2500	0.470(2)	0.0122
O6	0.2146(3)	0.0877(2)	0.072(1)	0.0095
N1	0.4631(2)	0.1824(1)	0.2839(6)	0.0039
C1	0.5728(3)	0.1294(2)	−0.0161(9)	0.0084
C2	0.4836(2)	0.1284(2)	0.1840(8)	0.0038
C3	0.3782(3)	0.1893(2)	0.4727(9)	0.0112
C4	0.3907(4)	0.2500	0.626(1)	0.0098
H31	0.3033(5)	0.1892(4)	0.377(2)	0.0203
H32	0.3757(6)	0.1497(4)	0.601(2)	0.0237
H41	0.3328(9)	0.25	0.785(3)	0.0201
H42	0.4673(9)	0.25	0.718(3)	0.0233
H43	0.6575(6)	0.0157(4)	0.344(2)	0.0197
H44	0.5989(5)	−0.0420(4)	0.450(2)	0.0224
H51	0.6662(6)	0.2848(5)	0.577(2)	0.0178
H61	0.1958(6)	0.0891(4)	−0.098(2)	0.0312
H62	0.2868(6)	0.0832(5)	0.087(2)	0.0331

[a] $U_{eq} = (1/3)\Sigma_i\Sigma_j U_{ij} a_i \cdot a_j$.

(26) Kahn O., Pei Y., Verdaguer M., Renard J. P., Sletten J. *J. Am. Chem. Soc.* **1988**, *110*, 782.

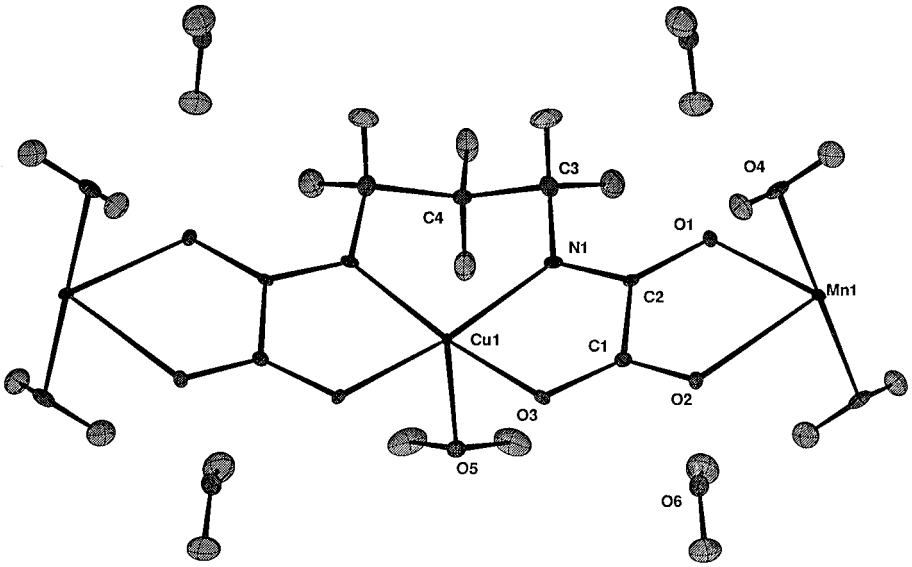

Figure 2. Structure of a section of chain for $MnCu(pba)(H_2O)_3 \cdot 2H_2O$, along with the atom labeling scheme. Anisotropic thermal ellipsoïds are drawn.

at the local spin density level, the VWN-functional was used.[31a] A nonlocal perturbation correction using the Becke-Perdew functional was emplyed on the final LSD-SCF density.[31b,c] A double-ζ split-valence plus polarization basis set optimized for DFT calculations, DZVP, was employed.[32] The contracted basis sets had the following composition: H [2s]; C, N, O [3s,2p,1d]; Cu, Mn [5s,3p,2d]. In the DMol-DSolid program the Perdew and Wang functional was used.[33] A DND basis was employed including double numerical basis set for all valence electrons and d-polarization functions for C, N, and O.

Description of the Nuclear Structure at 10 K

The values of the lattice parameters at 10 K are reported in Table 3 and are compared to the values at room temperature. The *a* and *c* parameters decrease from room temperature down to 10 K, while the *b* parameter increases. In Table 3 are also reported some selected bond lengths as well as the intra- and interchain metal−metal distances, both at room temperature and 10 K. The main features of the room temperature structure are retained at low temperature, but the chains become more elongated and come closer to each other. The bond lengths associated with the bridging network become all slightly longer at low temperature. This leads to a small increase of the Mn−Cu intrachain distance, from 5.412 to 5.431 Å. This trend is associated with the increase of the *b* parameter along which the chains run. The shortest interchain metal−metal separation, along the *a* axis direction, decreases from 5.211 to 5.154 Å as the temperature is lowered from room temperature down to 10 K. The manganese environment becomes less distorted because of the shortening of the Mn−O4 bond length, while the Mn−O1 and Mn−O2 bond lengths increase. This is not the case for the copper environment as the three Cu−O bond lengths increase at low temperature.

The atomic positions and equivalent isotropic displacements U_{eq} are given in Table 4, and the anisotropic thermal parameters U_{ij} are given as Supporting Information. A part of the chain framework at 10 K is represented in Figure 2.

Polarized Neutron Diffraction and Spin Density Maps

Polarized neutron diffraction was applied in order to determine the experimental magnetic structure factors F_M which are the Fourier components of the spin density.[34] The induced spin density in the unit cell was reconstructed from the F_M data set, using the same multipole model refinement as in ref 19. The Slater radial functions are also the same as in ref 19. The radial expansions were refined only for the manganese and copper atoms.

As in ref 19, the multipole description of the spin density was limited in a first refinement (I) to a spherical approximation for all the atoms. In a second refinement (II) the spin density located on the copper atom was restrainted to arise from a x^2-y^2 type orbital pointing from the metal atom toward the oxygen and nitrogen atoms located in the basal plane. The restraints on the copper multipole populations are described in ref 19.

The characteristics and results of the multipole refinements are reported in Table 5. The refinements were carried out on reflections with $F_M > 2\sigma(F_M)$. A total number of 228 reflections was used in the data refinement. This number includes 65 unique reflections of the first set and 163 unique reflections of the second set, with 30 reflections common to the two sets. A scaling factor was refined between the two sets of experimental magnetic structure factors. The spherical refinement (I) leads to an agreement factor $R_w(F_M)$ of 0.058. The application of a constraint on Cu in refinement (II) improves only very slightly the reliability factors as shown in Table 5.

The total induced moment per MnCu unit is given by the sum of the monopole populations before normalization. The moment of 3.2(1) μ_B derived from refinement (II) is somewhat lower than the measured magnetization at 10 K under 50 kOe, 3.6 μ_B. The spin populations obtained by normalization of the monopole populations to a moment of 4 μ_B are reported in Table 5. Let us note at this stage that the Mn and Cu radial exponents do not significantly deviate from the Slater exponents taken from the litterature[35] ($\zeta_{Mn} = 7.02$ ua^{-1} and $\zeta_{Cu} = 8.8$ ua^{-1}).

(27) DGauss included in *UniChem 2.3*; Cray Research, Inc.: 2360 Pilot Knob Road, Mendota Heights, MN 55120, 1994.
(28) Andzelm, J.; Wimmer, E. *J. Chem. Phys.* **1992**, *96*, 1280.
(29) DMol 2.3.7 and DSolid 2.3.7; Biosym Technologies Inc.: San Diego.
(30) Delley, B. *J. Chem. Phys.* **1990**, *92*, 508; *Phys. Chem.* **1996**, *100*, 6107.
(31) (a) Vosko, S. H.; Wilk, L.; Nusair, M. *Can. J. Phys.* **1980**, *58*, 1200. (b) Becke, A. D. *Phys. Rev. A* **1988**, *38*, 3098. (c) Perdew, J. P. *Phys. Rev. B* **1986**, *33*, 8822.
(32) Godbout, N.; Salahub, D. R.; Andzelm, J.; Wimmer, E. *Can. J. Chem.* **1992**, *70*, 560.
(33) Perdew, J. P.; Wang, Y. *Phys. Rev. B* **1992**, *45*, 13244.
(34) Brown P. J., Forsyth J. B.; Mason R. *Phil. Trans. R. Soc. Lond.* **1980**, *B290*, 481.
(35) Clementi, E.; Raimondi, D. L. *J. Chem. Phys.* **1963**, *38*, 2686. Hehre, W. J.; Stewart, R. F.; Pople, J. A. *J. Chem. Phys.* **1969**, *51*, 2657.

Table 5. Model Refinements: Reliability Factors, Radial Coefficients and Spin Populations (Normalized to 4 μ_B)

Refinement Conditions and Reliability Factors[a]		
no. of reflcns N_o	228	
refinement no.	I	II
no. of parameters N_v	13	13
$R_w(F)$	0.067	0.064
S	2.04	1.94
scaling factor between the two sets of data	1.132(10)	1.133(9)

Indexes n_l and Slater Exponents ζ (ua^{-1})			
	n_l	ζ	ζ
Mn	4	6.96(4)	6.96(3)
Cu	4	8.3(2)	9.3(2)
O	2	4.5	4.5
N	2	3.9	3.9
C	2	3.44	3.44

Spin Populations (in μ_B)		
Mn	4.93(3)	4.93(3)
Cu	−0.77(2)	−0.75(2)
O1	0.02(1)	0.02(1)
O2	0.01(1)	0.01(1)
O4	0.03(1)	0.02(1)
O3	−0.04(1)	−0.05(1)
N1	−0.07(2)	−0.08(2)
O5	0.01(2)	0.01(2)
C1	−0.03(2)	−0.03(2)
C2	−0.03(2)	−0.03(1)

[a] Same definition as in Table 1, with a weighting scheme $w = (1/\sigma^2)$.

The induced spin densities were drawn using the unnormalized multipole populations and the radial exponents obtained in refinement (II). The spin density maps projected along two perpendicular directions are presented in Figures 3 and 4, respectively. The former direction is perpendicular to the copper basal plane, and the latter direction is within this copper basal plane.

The spin populations on the manganese and copper atoms are found as 4.93(3) and −0.75(2) μ_B, respectively. The spin populations on the oxygen atoms on the manganese side are all close to 0.02(1) μ_B. On the other hand, the spin delocalization from the Cu(II) ion is more pronounced toward the nitrogen than the oxygen atoms of the copper basal plane. The spin populations on N1 and O3 are found as −0.08(1) μ_B and −0.05(1) μ_B, respectively. No significant population is observed on the oxygen atom O5 occupying the apical position in the copper coordination sphere. Small negative populations are found on the bridging carbon atoms.

The sum of the spin populations on each metal and its neighbors is respectively equal to 5.05(7) μ_B for manganese and −1.05(10) μ_B for copper. The opposite signs reflect the antiferromagnetic nature of the intrachain interaction. The amount of spin delocalized from copper toward its oxygen and nitrogen nearest neighbors (−0.24(8) μ_B) is twice as large in absolute value than the amount of spin delocalized from manganese toward its oxygen nearest neighbors (0.12(8) μ_B). The transferred moment amounts 24% of the total moment relative to copper, while it amounts to only 2.4% of the total moment relative to manganese. This ability of the Cu(II) ion to favor spin delocalization has the noteworthy consequence that the nodal surface (of zero spin density) is closer to the manganese than to the copper atom. This nodal surface intersects the Mn−Cu direction at a point located at 2.03 Å from Mn and 3.40 Å from Cu.

Table 6. Calculated Mulliken Spin Populations (in μ_B) for the Model Compounds **1**−**5**

	DGauss					DMol
model	**1**	**2**	**3**	**4**[a]		**5** (chain)
S value	1/2	5/2	BS[b]	BS[b]		GS[c]
Mn		4.72	4.67		4.72	4.56
O4		0.04	0.03	(NH_3 ax)	0.03	0.03
O′4				(NH_3 ax)	0.03	
O1	0.02	0.04	0.01		0.02	0.02
O1′			0.04	(NH_3 eq)	0.02	
O2	0.02	0.04	0.01		0.02	0.02
O2′			0.05	(NH_3 eq)	0.03	
C1	−0.01	0.00	0.00		0.00	0.00
C2	0.00	0.00	0.00		0.00	0.00
N1	0.12	0.02	−0.08		−0.12	−0.08
N1′			−0.12	(NH_2)	−0.09	
O3	0.10	0.02	−0.06	(N2)	−0.12	−0.07
O3′			−0.12	(NH_2)	−0.09	
Cu	0.46		−0.42		−0.41	−0.42
O5	0.00		0.00			0.00

[a] From ref 19. [b] Broken symmetry state, thus not an exact spin state. [c] Ferrimagnetic ground state.

Density Functional Theory Approach

In our DFT calculations five different model compounds were considered, namely (i) the mononuclear Cu and Mn fragments, **1** and **2**, respectively; (ii) a binuclear oxamato-bridged MnCu fragment **3**; (iii) the oxamido-bridged species **4** studied previously;[19] and (iv) finally, a chain compound **5** with the actual crystal structure (the noncoordinated water molecules were omitted), treated with periodic boundary conditions with gamma points sampling of the Brillouin zone. The results of the Mulliken spin population analysis are shown in Table 6.

Before discussing the DFT results, let us stress that there are some inherent problems comparing the spin populations recon-

Chart 1

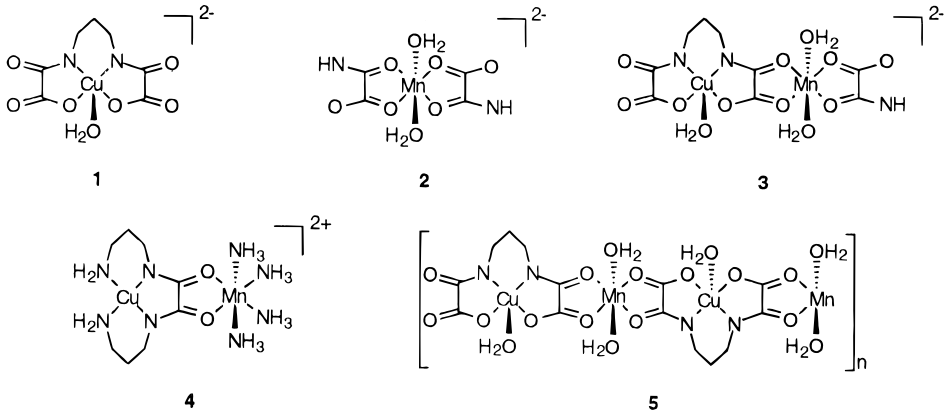

Table 7. Experimental Atomic Spin Populations (in μ_B) from Polarized Neutron Diffraction for the Chain and Pair Compounds

atom labeling chain/molecule			chain (this work)	pair (ref 19)
Mn			4.93(3)	4.32(2)
Cu			−0.75(2)	−0.47(1)
O1			0.02(1)	0.03(1)
O2			0.01(1)	0.03(1)
O4	/	N6	0.02(1)	0.08(1)
		N7		0.07(1)
		N5		0.09(1)
		N8		0.05(1)
O3	/	N2	−0.05(1)	−0.05(1)
N1			−0.08(1)	−0.05(1)
C1			−0.03(2)	−0.03(1)
C2			−0.03(1)	−0.03(1)
O5			0.01(2)	
		N3		−0.02(1)
		N4		−0.02(1)

structed from the experimental data and the theoretical spin populations. Indeed, the two sets of data are expressed using different basis sets. Moreover, we are faced with the problem of achieving the same spin state in the models as in the experiment.

For **1** the spin density is essentially delocalized toward the nitrogen and oxygen atoms of the basal plane bound to copper but also a little bit toward the peripheral oxygen atoms. As expected, no spin delocalization occurs toward the apical water molecule. For **2**, the spin delocalization toward the oxygen atoms bound to manganese is less pronounced. Models **3** and **4** can be used to compare oxamido and oxamato bridges. Although the electronic characteristics of the two bridges are close to each other, some differences may be observed, owing to two effects, namely the substitution of a nitrogen atom in the oxamido bridge by an oxygen atom in the oxamato bridge, and the nonplanarity of the bridging network in **3**. The discussion concerning **4** given in ref 19 remains valid for **3**, except that the nonplanarity of the bridging network decreases all the ferromagnetic interaction pathways, due to the nonorthogonality of the magnetic orbitals. For both **3** and **4** we also calculated the ground quintet−excited septet energy gap and found $3J = -553$ cm^{-1} for **3** and -710 cm^{-1} for **4**. As already pointed out,[19] the calculated values of the interaction parameters are much larger (in absolute value) than the experimental values; J was found to be equal to -23.4 cm^{-1} for the oxamato-bridged chain compound and -31.1 cm^{-1} for the oxamido-bridged pair compound. However, the calculated and experimental ratios J(oxamido)/J(oxamato) are close to each other. The DFT calculations reproduce the fact that the antiferromagnetic interaction is more pronounced through the oxamido than through the oxamato bridge.

With the possibility of periodic boundary conditions in the DMol-DSolid program we could also model the chain compound **5**. The DFT populations for the metal atoms are smaller (in absolute value) than the reconstructed experimental spin populations. We also note that the sums of the positive and negative spin populations obtained with the DMol-DSolid program, 4.72 μ_B and -0.72 μ_B, respectively, are lower than the experimental values, 5.05(7) μ_B and $-1.05(10)$ μ_B, respectively. This may be due to an overestimation of the overlap between the magnetic orbitals and the subsequent cancellation of spin densities. Significant negative spin populations are observed experimentally on the carbon atoms of the bridge. We think that a spin polarization of the C−O and C−N π-bonds is responsible for this, as outlined in ref 19. These negative spin populations on the carbon atoms of the bridge are not reproduced in the calculations, except for the mononuclear fragments; small spin populations of π-symmetry between -0.002 and $+0.005$ μ_B were found for **1** and **2**.

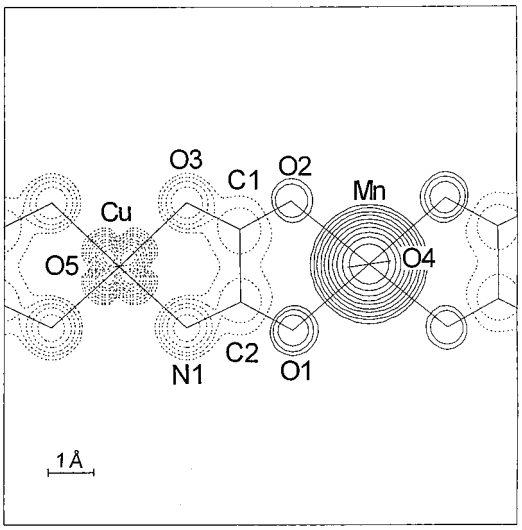

Figure 3. Induced spin density map for MnCu(pba)$(H_2O)_3$·$2H_2O$ at 10 K under 50 kOe in projection along the perpendicular to the copper basal plane. Solid lines are used for positive, and dashed lines for negative spin densities. Contours are $\pm 0.005 \times 2^{n-1}$ μ_B/Å^2 with n = 1, 2, ...

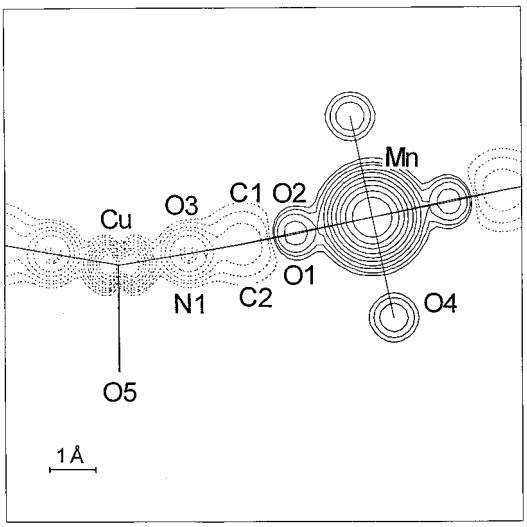

Figure 4. Induced spin density map for MnCu(pba)$(H_2O)_3$·$2H_2O$ at 10 K under 50 kOe in projection along the direction perpendicular to the previous direction within the copper basal plane.

Discussion and Conclusion

In this last section we would like to compare the spin density distributions for the MnCu binuclear compound previously investigated and the MnCu(pba)$(H_2O)_3$·$2H_2O$ ferrimagnetic chain. Before that, we must remind that the two bridging networks are not strictly identical; the bridge is an oxamido group in the former compound and an oxamato group in the latter compound. As a consequence, the two interaction parameters are somewhat different. The antiferromagnetic interaction is more pronounced through the oxamido group ($J = -31.1$ cm^{-1}) than through the oxamato group ($J = -23.4$ cm^{-1}). This difference results from two effects, namely (i) the Cu(II) magnetic orbital is more delocalized toward the nitrogen than the oxygen atoms of the copper basal plane and (ii) the Mn(oxamato)Cu bridging network of the chain is not strictly planar, which may also decrease the magnitude of the interaction.

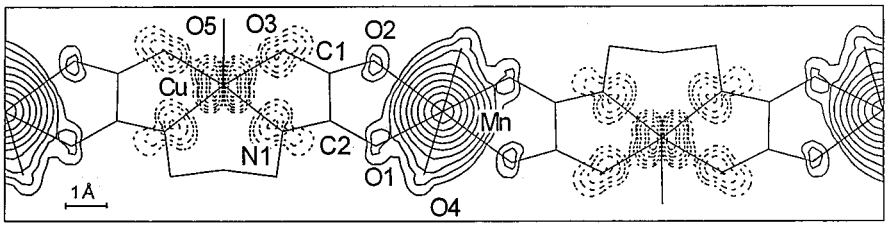

Figure 5. Calculated spin density map for $MnCu(pba)(H_2O)_3 \cdot 2H_2O$ using the DMol-DSolid DFT program in projection along the *c* crystallographic axis.

Let us successively discuss the similarities and the differences between the spin distributions for both the pair and the chain compounds. In both cases a large positive spin density is observed on the manganese side and a weak negative density on the copper side. This situation is the signature of the Mn(II)−Cu(II) antiferromagnetic interaction which leads to the ferrimagnetic behavior. The spin density is more diffuse on the copper than on the manganese side, so that the nodal surface is much closer to the manganese than the copper atom. For both compounds small negative spin populations are found on the bridging carbon atoms.

Let us now move on to the differences between binuclear and chain compounds. The most striking of these differences concerns the sums of positive and negative atomic spin populations, noted P_+ and P_-, respectively. For the pair compound P_+ was found as 4.67(8) μ_B, and P_- as −0.67(8) μ_B. These values exactly correspond to what is expected in a simple spin coupling description of the $S = 2$ ground state. In the chain compound P_+ is equal to 5.05(7) μ_B, and P_- to −1.05(10) μ_B. This difference between pair and chain compounds does not mean that the spin coupling description becomes less valid as the size of the system increases. In fact, it can be shown that for a ring chain system $(MnCu)_n$ a spin coupling description of the antiparallel spin ground state results in an increase in absolute value of P_+ and P_- as the number n of MnCu units increases. For instance, for $n = 2$, writing down the spin coupling wave function for the $S = 4$ ground state is still tractable; this wave function leads to $P_+ = 4.80\ \mu_B$ and $P_- = -0.80\ \mu_B$. As n tends to the infinite, the system gets very close to a Neel state with $P_+ = 5\ \mu_B$ and $P_- = -1\ \mu_B$.

Another difference between pair and chain compounds concerns the spin delocalization on both the manganese and copper sides. This spin delocalization is more important for the pair than for the chain compound. For the pair, the Mn(II) ion carries 92.5% of the positive spin density and the Cu(II) ion 70.1% of the negative spin density. These values are 97.6% and 76.0%, respectively, for the chain compound. It is difficult to say to what extent this situation is due to the differences of topology, pair versus chain, and to the fact that the environments of the metal ions are not identical in both compounds. Let us also remind that the chain is neutral, while the MnCu pair is a dication.

As a conclusion, we would like to emphasize that the spin density map is probably the description of the ground state for a molecular magnetic system which provides the largest amount of information on the magnetic phenomena. In a near future, we will report on new results of this kind.

Acknowledgment. We thank the Commissariat à l'Energie Atomique (CEA) for the use of the CRAY-C94 supercomputer in Grenoble. L.Ö. gratefully acknowledges a postdoctoral fellowship from the Swedish Research Council for Engineering Sciences and the Swedish Institute for funding. Dr. J. M. Mouesca is thanked for valuable discussion.

Supporting Information Available: List of anisotropic thermal parameters U_{ij} deduced from unpolarized neutron diffraction at 10 K (1 page). See any current masthead page for ordering and Internet access instructions.

JA9641620